A Model for Predicting Capacity Fade due to SEI Formation in a Commercial Graphite/LiFePO$_4$ Cell

A Model for Predicting Capacity Fade due to SEI Formation in a Commercial Graphite/$LiFePO_4$ Cell

Henrik Ekström[z] **and Göran Lindbergh**

Department of Chemical Engineering and Technology, Applied Electrochemistry, KTH, Stockholm, Sweden

An aging model for a negative graphite electrode in a lithium-ion battery, for moderate currents up to 1C, is derived and fitted to capacity fade experimental data. The predictive capabilities of the model, using only four fitted parameters, are demonstrated at both 25°C and 45°C. The model is based on a linear combination of two current contributions: one stemming from parts of the graphite particles covered by an intact microporous solid-electrolyte-interface (SEI) layer, and one contribution from parts of the particles were the SEI layer has cracked due to graphite expansion. Mixed kinetic and transport control is used to describe the electrode kinetics.

 [DOI: 10.1149/2.0641506jes] All rights reserved.

Manuscript submitted December 19, 2014; revised manuscript received February 6, 2015. Published March 10, 2015.

Lithium-ion batteries are used in all sorts of electric devices such as mobile phones, lawn mowers, electrical scooters and electric cars. Common for all lithium-ion battery chemistries is that they suffer from aging phenomena over time. Degradation occurs during storage, but is further induced by battery cycling and higher temperatures. Life time degradation generally occurs due to various processes such as electrolyte decomposition, loss of active material and loss of cycleable lithium due to parasitic reactions.[1]

The most common negative electrode material in lithium-ion batteries is graphite. For cells deploying negative graphite electrodes, significant amounts of cycleable lithium is lost into forming the solid-electrolyte-interface (SEI) layer on the graphite surface. The initial SEI formation during the first "formation" cycles of the battery is most pronounced, but, depending on operation conditions, the SEI layer formation will continue during the whole lifetime of the battery. The SEI layer is not homogeneous, neither with regards to morphology nor composition. Cracks are known to form upon battery cycling,[2] and various chemical compounds have been observed.[2,3] Experimental work has shown that for low currents (≤C/10) the long term capacity loss usually follows a $t^{1/2}$ dependence, and models in literature usually ascribes this dependence to a diffusion limitation through the SEI layer of a reacting species in the electrolyte that participates in forming the SEI layer.[4–6]

This paper focuses on SEI formation on graphite at moderate load currents (≤1C) at both 25°C and 45°C. For these conditions it has been shown that the SEI formation is the main cause of battery degradation.[7] Although not treated explicitly, the positive electrode material is assumed to be $LiFePO_4$ (LFP) since it has been seen that this positive electrode material does not suffer from nor cause significant degradation at these conditions.[8]

The experimental data used in this paper for parameter fitting, and testing of the predictive capabilities of the model, stems from a paper by Delacourt and Safari[9] in which a number commercial 2.3 Ah graphite/LFP cells, subject to different cycling schemes and temperatures, were monitored during a year with regards to the capacity fade.

Model and Simulations

Model assumptions.— There are numerous models in the literature implementing various aging phenomena in lithium-ion batteries.[10] Life-time simulations of lithium-ion batteries are commonly performed using physics-based models, and by estimation of relevant parameters such models have been able to narrow down the number of possible degradation mechanisms.[10–19] Typically these models contain expressions based on the physical model assumptions, sometimes mixed with some empirical expressions, and in some cases the models have been reduced to solely a number of empirical expressions. The aim of the physics-based model presented in this paper is to be able to predict aging of the battery using a minimum of parameters. Using a minimum set of parameters, the model should still capture the governing fundamental degrading processes in the negative electrode, for the range of operating conditions we are investigating. It should also be possible to apply the degradation model, with the fitted parameters presented derived in this paper, directly into more advanced battery performance models to, for instance, investigate spatial distribution degradation effects within the porous electrodes.

For the description of the battery main reaction, a single particle approach, which neglects spatial variations in potential and electrolyte concentration within the porous electrode, is used since it has been shown that such models can accurately describe the experimentally observed capacity fade under these conditions.[6, 10] Further, the solid-lithium concentration within the electrode particles is also assumed to be uniform. The above assumptions are all motivated from the fairly low battery currents used in the experiments. The battery cycling is made in galvanostatic mode, and hence the positive electrode and the separator need not be included in the model.

Earlier models have shown that the long term $t^{1/2}$ capacity fade behavior can be explained by diffusion limitations of a reacting species, transported through a SEI layer of increasing thickness.[4,5] However, since the experimental data indicated the capacity fade to be dependent on the battery state-of-charge (SOC), this model assumes that the parasitic SEI forming reactions are under mixed transport and electrokinetic control. The current expression for the SEI forming reaction assumes a cathodic Tafel equation, in combination with an expression for the limiting current due to diffusion through the SEI layer, using first order electrolyte solvent decomposition kinetics and linear solvent diffusion. The limiting current is hence proportional to the loss of lithium inventory.

For the SEI layer transport we propose a model based on a combination of transport though micro and macropores as depicted in Figure 1. The micropores are present at all times, whereas the macropores are formed upon expansion of the graphite particle. By this model the SEI layer formation currents becomes a linear combination from two contributions: one SEI forming current for on the parts of the graphite particles were the microporous SEI layer is intact and covering, and one contribution stemming from the parts of the graphite particles above which the macropores (cracks) have formed due to graphite expansion. A constant microporosity is ascribed to the covering layer whereas the volume fraction of the cracked SEI layer is assumed to depend on the graphite expansion rate, which in turn depends both on the intercalation current and SOC. During charge, when the graphite expands, a linear dependence between the volume fraction of the cracks and the graphite volume expansion rate is used, whereas the volume fraction is set to zero during discharge, implying that the

[z]E-mail: heek@kth.se

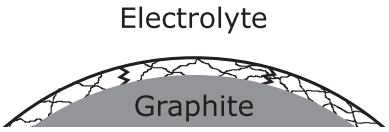

Figure 1. Cracks (macropores) formed in the microporous SEI layer due to expansion of the graphite particle during charge of the graphite electrode. The cracks enhance transport of the SEI layer forming species. The SEI layer is located between the graphite and the electrolyte.

cracks are immediately closed during open circuit or discharge, and that the SEI reconfigures to an intact layer of homogeneous thickness and microporosity.

We here note that our model approach for describing the impact of cracking on the SEI layer should be seen as semi-empiric and quite rudimentary, especially the linear relation between the macropore volume and the graphite expansion rate. Another admittedly coarse simplification in our model is, although we use different kinetic expressions for the macropores and the micropores, that the resulting SEI contributes uniformly to form the microporous layer, something that may only be motivated when seen as an average behavior over multiple charge-discharge cycles. A more advanced model would need to integrate the macropore expansion and contraction over time, and also incorporate the effect of the local SEI deposition within the expanding pores, which would induce hysteresis effects depending on the cycling history. Such a more elaborate model, able to capture the transient behavior of the changes in porosity during the different stages of a single charge-discharge cycle, would however increase computational load and the number of unknown parameters that would have to be fit to experimental data.

Mathematical model for SEI formation.— A list of the symbols and indexes used in the model are shown in Tables I and II, respectively.

The model is zero-dimensional and defines the accumulated charge of lithium, Q_{SEI} (C), lost in the battery due to side reactions forming the SEI layer on the graphite particles.

The charge balance is defined as

$$\frac{\mathrm{d}Q_{\mathrm{SEI}}}{\mathrm{d}t} = -I_{\mathrm{SEI}} \quad [1]$$

where I_{SEI} (A), is the current of the parasitic SEI forming reactions.

The SEI layer thickness, s, is proportional to Q_{SEI} according to

$$s = \frac{Q_{\mathrm{SEI}} V}{(1-\varepsilon_{\mathrm{cov}})A} \quad [2]$$

where $\varepsilon_{\mathrm{cov}}$ is the porosity of the microporous part of the SEI layer, A (m^2) is the surface area of the graphite particles, F (96485 C/mol) is Faraday's constant and V (m^3/C) is the coulombic volume of the SEI layer (formed SEI layer volume per passed charge of the reaction).

I_{SEI} is defined as

$$I_{\mathrm{SEI}} = I_{\mathrm{cov}} + I_{\mathrm{crd}} \quad [3]$$

where I_{cov} (A) represents current contributions from the surfaces of the graphite particles that are covered by the intact microporous SEI layer, and I_{crd} (A) represents current contributions from surfaces of graphite particles where the SEI layer has cracked due to expansion of the graphite particles.

The expressions for I_{cov} and I_{crd} are both derived similarly, assuming a first order mass transport limiting current through a Nernst boundary layer

$$I_i = \frac{I_{\mathrm{kin},i}}{1 + \frac{I_{\mathrm{kin,i}}}{I_{\mathrm{lim},i}}} \quad [4]$$

where i is an index representing either covering (cov) or cracked parts (crd) of the SEI layer, $I_{\mathrm{kin},i}$ (A) is the kinetic current (in the absence of mass transport limitations), and $I_{\mathrm{lim},i}$ (A) is the maximum current of the SEI forming reaction due to mass transport limitations.

Table I. Symbols used in the model.

Symbol	Unit	Description
a_{crd}	1	Proportionality factor
A	m^2	Electrode surface area
c	$\mathrm{mol/m}^3$	Bulk concentration
C_{batt}	1	Relative battery capacity
D_i	m^2/s	Diffusion coefficient
$E_{\mathrm{eq},i}$	V	Equilibrium potential
f	1	Lumped fitting parameter
F	C/mol	Faraday's constant, 96485 C/mol
i	-	Index, see Table II.
I_0	A	Exchange current
$I_{1\mathrm{C}}$	A	1C charge/discharge current, 2.3 A
I_i	A	Current
$I_{\mathrm{kin},i}$	A	Kinetic current
$I_{\mathrm{lim},i}$	A	Limiting current
I_{load}	A	Battery load current
J	1	Lumped fitting parameter
H	1	Lumped fitting parameter
k_{ical}	V	Proportionality factor
K_{crd}	1	Expansion factor
$Q_{\mathrm{batt},0}$	C	Initial battery capacity, 2.3 Ah
Q_{neg}	C	Charge stored in the negative graphite electrode
Q_{SEI}	C	Charge lost to SEI forming reactions
R	J/(mol K)	Molar gas constant, 8.1345 J/(mol K)
s	m	SEI layer thickness
$\mathrm{soc}_{\mathrm{batt}}$	1	Battery state-of-charge
T	K	Temperature
V	m^3/C	Coulombic volume for forming the SEI layer
x	1	Stoichiometric coefficient in $\mathrm{Li}_x\mathrm{C}_6$
α	1	Transfer coefficient
ε_i	1	Volume fraction (porosity)
η_i	V	Overpotential
ϕ_s	V	Potential, electrode phase
ϕ_l	V	Potential, electrolyte phase
τ_i	1	Tortuosity

The kinetic current for the covered areas is assumed to follow an irreversible cathodic Tafel expression according to

$$I_{\mathrm{kin,cov}} = -\varepsilon_{\mathrm{cov}} I_0 \exp\left(-\frac{\alpha \eta_{\mathrm{SEI}} F}{RT}\right) \quad [5]$$

where I_0 (A) is the exchange current, α (1) is the cathodic transfer coefficient, η_{SEI} (V) is the overpotential of the SEI forming reaction, R (8.1345 J/(mol K)) is the molar gas constant and T (K) is the battery temperature.

Arbitrarily setting the equilibrium potential of the SEI reaction, $E_{\mathrm{eq,SEI}}$ (V), to zero and grounding the electrode phase potential ϕ_s (V), the overpotential is defined as

$$\eta_{\mathrm{SEI}} = \phi_s - \phi_l - E_{\mathrm{eq,SEI}} = -\phi_l \quad [6]$$

where ϕ_l (V) is the electrolyte phase potential.

The electrolyte phase potential is related to the equilibrium potential of the intercalation reaction, $E_{\mathrm{eq,ical}}$ (V), and the the corresponding

Table II. Indices for index *i* in Table I.

Index	Description
cov	Areas covered by an microporous SEI layer
crd	Areas where the SEI layer has cracked
ical	Intercalating reaction
neg	Negative electrode
SEI	SEI layer, or SEI layer forming reaction

overpotential, η_{ical} (V), according to

$$\phi_l = -\left(E_{eq,ical} + \eta_{ical}\right) \quad [7]$$

Assuming a transfer coefficient of 0.5 for the intercalating reaction and inverting the Butler-Volmer equation, the following relation between the intercalation current and the overpotential is used

$$\eta_{ical} = \frac{RT}{0.5F}\text{arcsinh}\left(\frac{I_{ical}}{2k_{ical}I_{1C}((1-x)x)^{0.5}}\right) \quad [8]$$

where x (1) is the stoichiometric coefficient for lithium in Li_xC_6 in the graphite electrode, I_{ical} (A) is the intercalation current into the graphite particles, I_{1C} (A) is the battery nominal 1C charge current and k_{ical} (1) is a proportionality constant chosen to render an overpotential of 20 mV at $I_{ical} = I_{1C}$ and $x = 0.5$.

The kinetic current expression for the graphite particle surfaces where the SEI layer has cracked is written similarly as for the covered areas so that

$$I_{kin,crd} = -\varepsilon_{crd}I_0\exp\left(-\frac{\alpha\eta_{SEI}F}{RT}\right) \quad [9]$$

where ε_{crd} is the volume fraction of the cracks in the SEI layer. ε_{crd} is assumed to be proportional to the expansion rate of the graphite particles according to

$$\varepsilon_{crd} = a_{crd}K_{crd} \quad [10]$$

where a_{crd} (1) is a dimensionless proportionality factor and K_{crd} (1) is an expansion factor defined as

$$\begin{aligned} K_{crd} &= -2\tfrac{I_{ical}}{I_{1C}} && I_{ical} < 0 \text{ and } x < 0.3 \\ K_{crd} &= 0 && I_{ical} < 0 \text{ and } 0.3 \le x \le 0.7 \\ K_{crd} &= -\tfrac{I_{ical}}{I_{1C}} && I_{ical} < 0 \text{ and } x > 0.7 \\ K_{crd} &= 0 && I_{ical} \ge 0 \end{aligned} \quad [11]$$

The expansion factor dependence on x is an estimation based on experimental data for graphite expansion,[20] with support from theoretical calculations.[21] K_{crd} is only being non-zero when the graphite particles expand due to lithium intercalation.

By the assumption of a Nernst boundary layer, the limiting current density is defined to be inversely proportional to the accumulated SEI layer thickness so that we for the covering parts get

$$I_{lim,cov} = -\frac{\varepsilon_{cov}cD_{cov}FA}{s} \quad [12]$$

where c (mol/m^3) is the bulk concentration of SEI forming reactant in the electrolyte and D_{cov} (m^2/s) is the diffusion coefficient in the covering layer.

Similarly for the cracked parts we get

$$I_{lim,crd} = -\frac{\varepsilon_{crd}cD_{crd}FA}{s} \quad [13]$$

where D_{crd} (m^2/s) is the diffusion coefficient in the cracked diffusion layer.

The diffusion coefficients D_{cov} and D_{crd} are related to the tortuosity, τ_i (1), of the micropores or cracks according to

$$D_i = \frac{D}{\tau_i} \quad [14]$$

where D is the diffusion coefficient for the reacting electrolyte species in the free electrolyte phase.

Lumped fitting parameters.— Three lumped parameters can be derived from the model. First, for the covering parts we define a non-dimensional exchange current, J (1),

$$J = \frac{\varepsilon_{cov}I_0}{I_{1C}} \quad [15]$$

and a frequency parameter, f (1/s),

$$f = \frac{\tau_{cov}VI_{1C}^2}{\varepsilon_{cov}(1-\varepsilon_{cov})cDFA^2} \quad [16]$$

Table III. Summary of simulations performed. All simulations were performed at both 25°C and 45°C. Equation 1 is a charge balance ordinary differential equation (ODE) for the SEI formation. Equation 23 is only used to assess the battery state-of-charge vs time during cycling since this experimental data was not available.

Cycling Mode	ODEs solved	Purpose
OCP	1	least square fitting of parameters α, J, f
1C CC cycling	1 and 23	least square fitting of parameter H
complex cycling	1 and 23	test predictive capabilities (no parameter fitting)

and hence get

$$I_{cov} = -\frac{JI_{1C}}{\exp(\frac{\alpha\eta_{SEI}F}{RT}) + \frac{Q_{SEI}fJ}{I_{1C}}} \quad [17]$$

For the cracked parts, assuming $\tau_{crd} = \tau_{cov}$, and defining a non-dimensional relative expansion factor, H (1), as

$$H = \frac{a_{crd}}{\varepsilon_{cov}} \quad [18]$$

one gets

$$I_{crd} = HK_{crd}I_{cov} \quad [19]$$

so that

$$I_{SEI} = -(1 + HK_{crd})\frac{JI_{1C}}{\exp(\frac{\alpha\eta_{SEI}F}{RT}) + \frac{Q_{SEI}fJ}{I_{1C}}} \quad [20]$$

Simulations and battery life time predictions.— A brief summary of the simulations performed is shown in Table III. All model simulations were made in Comsol Multiphysics, version 5.0.0.244 using the BDF time-dependent solver. Parameter fitting was made by use of the Levenberg-Marquardt optimization solver using numerical gradients of the second approximation order. Battery cycling was accomplished using the Events interface.

All simulations solved for the SEI charge balance Equation 1. Since the model only takes lithium loss due to SEI formation into consideration, the relative battery capacity, C_{batt} (dimensionless), was calculated as

$$C_{batt} = \frac{Q_{batt,0} - Q_{SEI}}{Q_{batt,0}} \quad [21]$$

The initial value for Q_{SEI} was set to 0 at $t = 0$, corresponding to an initial capacity of 100%.

Experimental data[9] for two different temperatures, 25°C and 45°C, was used for parameter fitting of two different sets of the transfer coefficient α and the three lumped parameters J, f, H, one set for each temperature. Data for 12 months was available, but for the cycling at 45°C, only data for the first six months was used since the authors reported loss of active material after six months — a phenomena not included in the model.

The equilibrium potential of the lithium insertion reaction, depending on the SOC of the negative electrode (x in Li_xC_6), was based on experimental data as reported by the same authors.[9]

The fitting was conducted in two steps. In the first step, α, J and f were fitted to the capacity fade experimental data for when the battery was aged at open circuit at constant SOC, soc_{batt}(1), of either 50% or 100%. In these experiments the battery was only cycled once after 1, 3, 6, 9 and 12 months to monitor the battery capacity and to re-establish the SOC to the desired level.

In these open circuit simulations, soc_{batt} was taken from the reported data. The cell was assumed to be limited by the positive electrode capacity, with the total capacity of the negative active material

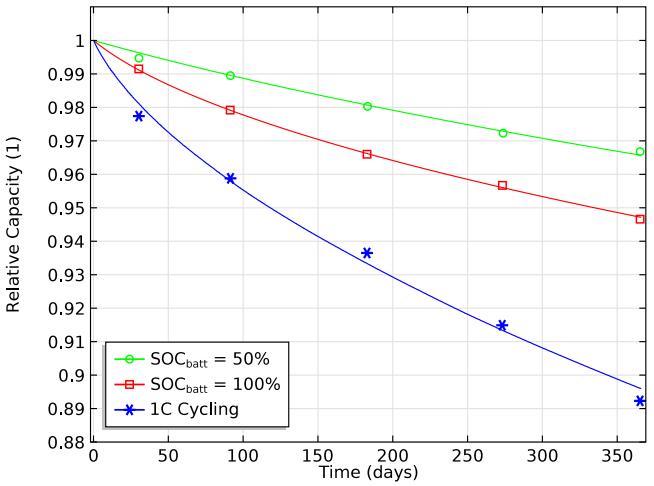

Figure 2. Fitted model simulation results (solid lines) at $T = 25°C$ and corresponding experimental data (markers) of relative battery capacity vs time for open circuit at 50% SOC (green, circles), open circuit at 100% SOC (red, squares) and constant charge-discharge 1C cycling (blue, asterisks).

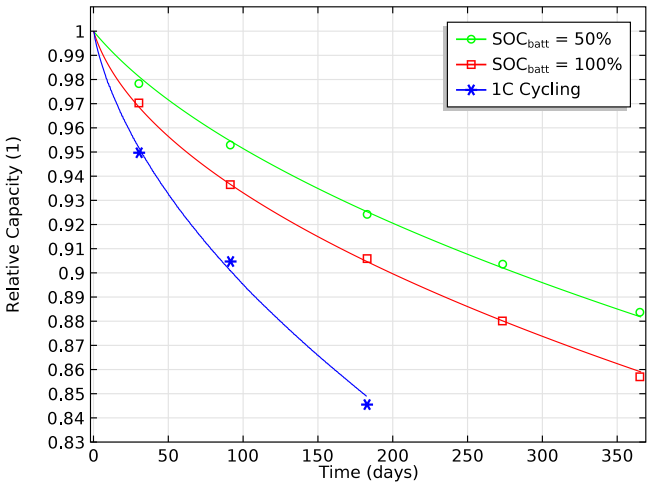

Figure 3. Fitted model simulation results (solid lines) at $T = 45°C$ and corresponding experimental data (markers) of relative battery capacity vs time for: open circuit at 50% SOC (green, circles), open circuit at 100% SOC (red, squares) and constant charge-discharge 1C cycling (blue, asterisks).

assumed to be 125% of the initial battery capacity, so that

$$x = \frac{\text{SOC}_{\text{batt}}}{1.25} \quad [22]$$

In a second step, H was fitted versus cycling data where a constant charge-discharge 1C scheme was used, including a 30 minutes resting period between each charge and discharge period. Also in these experiments, the battery was monitored with regards to capacity fade with same intervals as for the SOC experiments.

For the cycling simulations, explicit data for the state of charge vs time was not available, instead an extra charge balance equation was added to solve for the charge, Q_{neg} (C), stored as solid lithium in the negative graphite electrode of a lithium-ion battery electrode according to

$$\frac{\text{d}Q_{\text{neg}}}{\text{d}t} = -I_{\text{ical}} = I_{\text{load}} + I_{\text{SEI}} \approx I_{\text{load}} \quad [23]$$

where I_{load}(A) is the time dependent battery load current, and x was calculated according to

$$x = \frac{Q_{\text{neg}}}{1.25 Q_{\text{batt,0}}} \quad [24]$$

where $Q_{\text{batt,0}}$ (2.3 Ah) is the nominal battery capacity. For the cycling simulations the initial value for Q_{neg} was 0.5.

After the parameter fitting, the model was tested, using the fitted parameter values, using a more complex cycling scheme and compared against the corresponding experimental data. The complex cycling scheme included one longer duration consisting of 5 s short steps, one longer C/2 charge period, and resting periods. The average charge and discharge rates during the short stepping duration were C/10 and C/2, respectively, with a ratio of the number of charging steps to the discharging steps being 38 to 159.

Results and Discussion

The fitted model results and corresponding experimental data for the open circuit and constant charge/discharge cycling for 25°C and 45°C are shown in Figure 2 and Figure 3, respectively. The fitted parameter values are shown in Table IV.

The fitted value of 0.69 and 0.67 for the transfer coefficient α for each temperature matches the value of 0.69 found by Delacourt and Safari when fitting a different model to the same data.[10]

Analyzing the fitted values of the lumped parameters is hard, given that these values represents the combined effect of a number of involved physical parameters. However, some remarks can be done. Firstly, J increases by a factor of 4 when going from 25°C to 45°C, which would correspond to an activation energy of 66 kJ/mol. This indicates a higher value for the exchange current, which is expected given the higher temperature, but an increased microporosity of the SEI layer may also contribute. Secondly, it is seen that f decreases by 80% when raising the temperature. This could partly be explained by a higher diffusion coefficient in as the temperature increases from 25°C to 45°C. Viscosity data from literature[22] in combination with the Stokes-Einstein equation would however predict the diffusion coefficient to increase only by 50%. The lower f value could hence also be an indication of an increase in the SEI layer microporosity (assuming the porosity to be lower than 50%). A third possible contribution would be a decrease in the coulombic volume of the product species forming the layer, i.e. that the net layer growth per passed charge in the parasitic reaction becomes lower at higher temperatures. This could be an indication of a change in the constitution of the actual SEI species being formed or an indication of consecutive dissolution of the SEI layer as it forms. The lowered H value for the higher temperature is an indication of a relatively smaller impact of the crack formation in relation to the overall capacity fade. This could be explained by a higher microporosity of the covering SEI layer.

Figure 4 shows the prediction simulation results for the complex cycling scheme, using the already fitted model parameter values as shown in Table IV. The corresponding experimental data is plotted in the same figure. As can be seen, the simulation results exhibit a fair match with the experimental data for this cycling scheme.

At 45°C the model underpredicts the capacity fade somewhat, with a growing discrepancy over time. The model presented in this paper assumes a fully developed diffusion layer within the SEI layer that forms instantly when the battery load current changes. However, when the cracks form due to changes in the battery load current, there will be a transition time for the diffusion layer establish, during which the parasitic SEI forming currents will be generally higher than estimated by the current model. At 45°C the SEI layer will be thicker and this effect would be more pronounced toward the end of the simulation. To

Table IV. Fitted parameter values for α, J, f and H.

Symbol	Unit	Value at $T = 45°C$	Value at $T = 45°C$
α	1	0.69	0.67
J	1	$1.9 \cdot 10^{-4}$	$8.4 \cdot 10^{-4}$
f	1/s	$1.1 \cdot 10^{3}$	$2.0 \cdot 10^{2}$
H	1	11	6.7

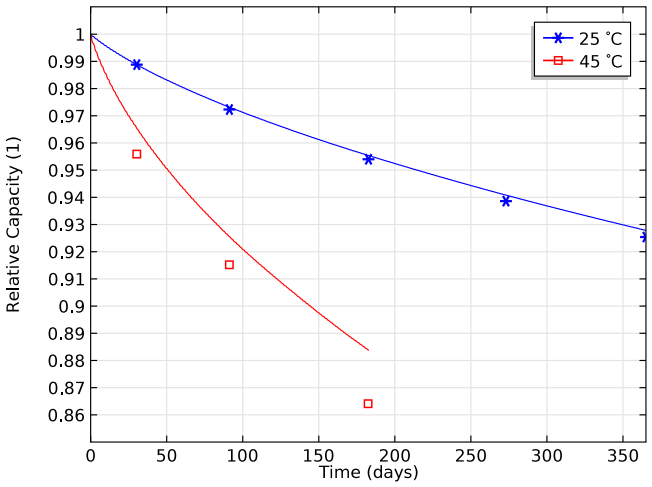

Figure 4. Simulation of a complex cycling scheme (solid lines) and corresponding experimental data (markers) at $T = 25°C$ (blue, asterisks) and $T = 45°C$ (red, squares).

fully describe this effect one would need to include a mass transport model for the SEI layer, which would introduce a number of additional parameters to the model.

Conclusions

In this paper we derived an aging model for moderate currents up to 1C for a negative graphite electrode in a lithium-ion battery. The model is based on a linear combination of two current contributions: one stemming from parts of the graphite particles covered by an intact microporous SEI layer, and one contribution from parts of the particles were the SEI layer has cracked. Mixed kinetic and transport control is used for the electrode kinetics.

Three derived lumped parameters together with the transfer coefficient of the parasitic reaction where fitted to capacity fade experimental data. Analysis of the fitted parameters indicate a higher kinetic activity for the SEI forming reaction at 45°C compared to 25°C and/or an increased SEI layer porosity. There are also indications of reduced SEI volume per passed charge of the SEI forming reaction for the higher temperature. The predictive capabilities of the model, using the fitted parameters, are fair at both 25°C and 45°C.

Acknowledgments

The financial support from the Swedish Hybrid Vehicle Centre (SHC) is gratefully acknowledged.

References

1. J. Vetter, P. Novák, M. Wagner, C. Veit, K.-C. Möller, J. Besenhard, M. Winter, M. Wohlfahrt-Mehrens, C. Vogler, and A. Hammouche, *J. Power Sources*, **147**, 269 (2005).
2. H.-L. Zhang, F. Li, C. Liu, J. Tan, and H.-M. Cheng, *The J. Phys. Chem. B*, **109**, 22205 (2005).
3. S. Malmgren, K. Ciosek, M. Hahlin, T. Gustafsson, M. Gorgoi, H. Rensmo, and K. Edström, *Electrochimica Acta*, **97**, (2013).
4. H. J. Ploehn, P. Ramadass, and R. E. White, *J. the Electrochem. Soc.*, **151**, 456 (2004).
5. A. J. Smith, J. C. Burns, X. Zhao, D. Xiong, and J. R. Dahn, *J. Electrochem. Soc.*, **158**, A447 (2011).
6. M. B. Pinson and M. Z. Bazant, *J. Electrochem. Soc.*, **160**, A243 (2013).
7. P. Liu, J. Wang, J. Hicks-Garner, E. Sherman, S. Soukiazian, M. Verbrugge, H. Tataria, J. Musser, and P. Finamore, *J. Electrochem. Soc.*, **157**, A499 (2010).
8. M. Klett, R. Eriksson, J. Groot, P. Svens, K. Ciosek Högström, R. W. Lindström, H. Berg, T. Gustafson, G. Lindbergh, and K. Edström, *J. Power Sources*, **257**, 126 (2014).
9. M. Safari and C. Delacourt, *J. Electrochem. Soc.*, **158**, A1123 (2011).
10. C. Delacourt and M. Safari, *J. Electrochem. Soc.*, **159**, A1283 (2012).
11. P. Arora, M. Doyle, and R. E. White, *J. Electrochem. Soc.*, **146**, 3543 (1999).
12. P. Arorat, R. E. White, S. Carolina, and M. Doyle, *J. Electrochem. Soc.*, **145**, 3647 (1998).
13. A. Awarke, S. Pischinger, and J. Ogrzewalla, *J. Electrochem. Soc.*, **160**, A172 (2013).
14. E. Prada, D. Di Domenico, Y. Creff, J. Bernard, V. Sauvant-Moynot, and F. Huet, *J. Electrochem. Soc.*, **160**, A616 (2013).
15. P. Ramadass, B. Haran, P. M. Gomadam, R. White, and B. N. Popov, *J. Electrochem. Soc.*, **151**, A196 (2004).
16. Y. Dai, L. Cai, and R. E. White, *J. Electrochem. Soc.*, **160**, A182 (2013).
17. L. Cai, Y. Dai, M. Nicholson, R. E. White, K. Jagannathan, and G. Bhatia, *J. Power Sources*, **221**, 191 (2013).
18. J. Vazquez-Arenas, M. Fowler, X. Mao, and S.-k. Chen, *J. Power Sources*, **215**, 28 (2012).
19. R. Narayanrao, M. M. Joglekar, and S. Inguva, *J. Electrochem. Soc.*, **160**, A125 (2013).
20. J. B. Siegel, A. G. Stefanopoulou, P. Hagans, Y. Ding, and D. Gorsich, *J. Electrochem. Soc.*, **160**, A1031 (2013).
21. Y. Qi, H. Guo, L. G. Hector, and A. Timmons, *J. Electrochem. Soc.*, **157**, A558 (2010).
22. H. Lundgren, M. Behm, and G. Lindbergh, *J. Electrochem. Soc.*, **162**, A413 (2015).